CHAPTER 2

TEXTURE ANALYSIS OF DUAL POLARIMETRIC C-BAND SAR DATA FOR LAND USE AND LAND COVER CLASSIFICATION

2.1 INTRODUCTION

Remote sensing technologies have been proved as an important approach to document, describe and enumerate LULC efficiently. The study of LULC is one of the important factors in forming policies concerning economic, demographic and environmental concerns from local to global level. For countries like India having varied climatic zone, land use planning using optical data has limitations because of frequent cloud cover. For such regions with its all-weathered capability, SAR data have been receiving considerable attention in the remote sensing community (Qi et al., 2012; Li et al., 2012; Chakraborty et al., 2013; Uhlmann and Kiranyaz, 2014; Zakeri et al., 2017).

The LULC classification of remote sensing images by different space-borne sensors has drawn a lot of interest (Lu and Weng, 2007; Dixon and Candade, 2008; Kumar et al., 2015) but cloud cover and weather conditions restrict the continuous observation. This issue may be overcome by using an important technique such as SAR for acquiring images of earth's surface in all weather and illumination conditions. Therefore, in the last few years, numerous studies have been attempted for LULC classifications using the potential of SAR data such as European Remote Sensing Satellite (ERS), SAR Satellite (SARSAT-1/2), Radar Imaging Satellite (RISAT-1), ALOS PALSAR (Rajesh et al., 2001; Li et al., 2012; Chakraborty et al., 2013; Uhlmann and Kiranyaz, 2014). The RISAT-1, with its launch on 26th April, 2012, became the first Indian space-borne hybrid polarimetric SAR system. It carries C-band

hybrid polarimetric SAR system that supports right circular transmit and coherent linear receive (CTLR) mode in addition to other standard modes and can be operated at various resolution and swath (Misra et al., 2013; Valarmathi et al., 2013).

In satellite image classification, texture features supplies valuable information for SAR data interpretation, so that it could differentiate various classes of terrain features (Sali and Wolfson, 1992; Lillesand et al., 2008). Herold et al., (2004) carried out a study to examine the usefulness of SAR-derived texture measures for identifying different land features. In general, a texture is referred to as the pattern of intensity variations in an image where the various LULC classes are not sufficiently distinguishable; it has become vital to improve LULC classification accuracy (Rajesh et al., 2001; Ndi Nyoungui et al., 2002). A number of texture features have been developed (Haralick et al. 1973; Rajesh et al. 2001), however the picking of appropriate texture features is still not obvious. The identification of suitable textural images is a challenging task due to textural variation as a function of the landscape of study area, selection of texture measure, moving window size and the image itself (Chen et al., 2004).

Several classification algorithms exist to classify LULC categories in remote sensing images (Lu and Weng 2007; Kumar et al. 2016a), however the selection of a suitable algorithm is still an important and complex task. The traditional MLC is the frequently used approach based on statistical theory (Richards and Jia, 2006). The MLC is employed for the interpretation and classification of satellite images but because of the limitations of normal distribution, other advanced non parametric algorithms are required and found extremely useful than the traditional parametric algorithms (Lu et al., 2004). In the past two decades, advanced classification algorithms for instance SVM, RF, and ANN have been used broadly

for classification of space-borne images (Kavzoglu et. al., 2003; Szuster et al., 2011; Shiraishi et al., 2014). ANN is a non-parametric classification algorithm (Lu and Weng, 2007) which is not influenced by the hypothesis of normal distribution of data and works on back propagation (BP) training algorithm (Dixon and Candade, 2008). It is used broadly for various applications by the remote-sensing community (Mas and Flores, 2008; Kumar et al., 2015; Mishra and Rai, 2016). Furthermore, ANN has been found in improving classification accuracy in comparison to pixel based method such as MLC (Mas and Flores, 2008; Pijanowski et al., 2002). Among the advanced classification algorithms, RF and SVM have received significant consideration because of numerous advanced image-handling capabilities. The RF is established to be superior to MLC in terms of classification accuracy for optical imagery (Rodriguez- Galiano et al., 2012). In addition, RF requires only just two parameters to be set; while the SVM requires several user-defined parameters. In spite of this, RF provides equally well classification results in comparison to SVM (Pal, 2005). The SVM is non-parametric classification algorithm based on machine learning theory (Vapnik, 1999). The performance of SVM has been found better in comparison to other classification methods (Dixon and Candade, 2008, Szuster et al., 2011; Kumar et al., 2015).

The present study is conducted to (1) explore the potential of dual polarimetric RISAT-1 SAR data at C-band for LULC classification, (2) recognize the polarization and texture features most appropriate for LULC classification, and (3) compare the performance of different classifiers; MLC, ANN, RF and SVM on RISAT-1 image classification.

2.2 STUDY AREA

A part of Varanasi district was chosen as study area for this work, having centre latitude 25°17′51.19″ N and longitude 82°56′36.74″ E. The map showing geographical

location of the chosen study area as viewed on RISAT-1 hybrid FCC image (*Red*-HV, *Green*-HH, *Blue*-HH+HV) are shown in Figure 2.1.

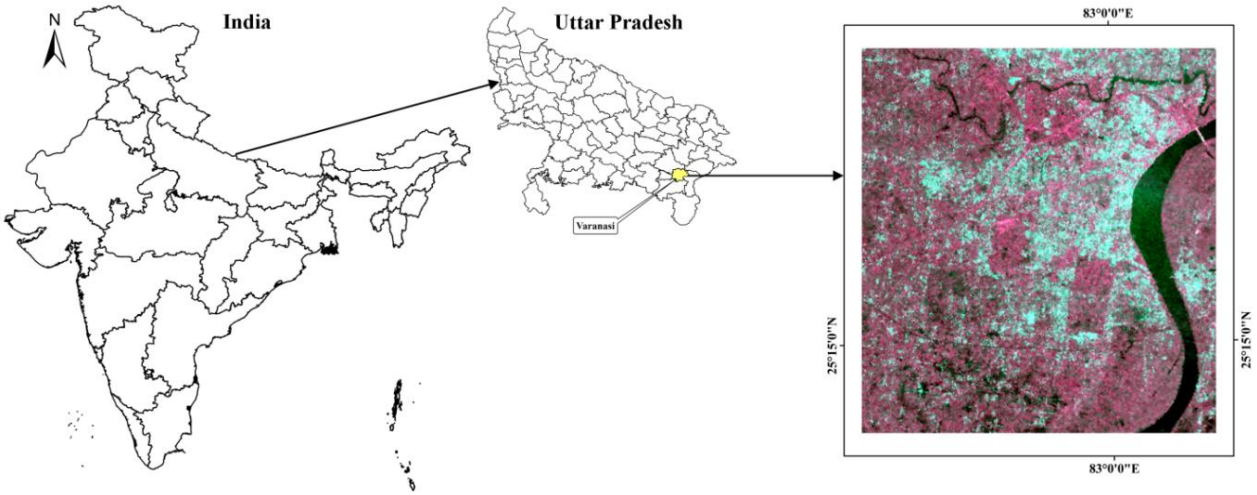

Figure 2.1 Location map of the study area as viewed on RISAT-1 hybrid FCC image (*Red*-HV, *Green*-HH, *Blue*-HH+HV)

2.3 MATERIALS AND METHODOLOGY

2.3.1 Field data collection and identification of LULC classes

The study area was visited to collect sample plots for each LULC class on the day of satellite image acquisition using a hand held GPS receiver. Six major LULC classes: agricultural land, dense vegetation, sparse vegetation, built up, fallow land and water bodies are identified according to the landscape of study area. During field observation, a total of 135 sample plots were selected and employed to create the respective region of interest (ROI) polygons using ENVI 5.1 image analysis software. One of these ROI files was used as training pixels and other as testing pixels. The training samples are selected randomly for various LULC classes using ROI tool available in ENVI software. The training samples are well allocated and represent the entire study area. These created ROIs were utilized to train the classifiers for classification purpose. In total, 4056 pixels were used as the training pixels, whereas 1352 pixels were employed as the testing pixels for all classification algorithms.

2.3.2 SAR data collection and preprocessing

The preprocessing of SAR data was carried out by using ENVI-SARscape (v5.1) image analysis software. In this study, RISAT-1 Medium-resolution ScanSAR (MRS) C-band (5.35 GHz) level 1 (L1) product with dual polarizations HH and HV (slant range, unsigned 16-bit, nominal incidence angle of 36.85°, 7.19 m pixel spacing) was used. It has also capability for imaging the earth's surface in different modes (Misra et al., 2013). The SAR image employed in the present work was acquired on 9th August 2013. The L1 data of RISAT-1 was first imported into SARscape and multi-looked 2 times in azimuth and 2 times in range direction.

The C- band SAR image was registered to a georectified Landsat 8-OLI image (UTM coordinate system, zone 44, North). For C-band SAR image, the RMSE was 1.159 pixels based on 11 control points. To facilitate the full use of original two polarizations HH and HV, a new band was produced as NB = HH+HV. With the aim of noticeable discrimination among various LULC classes, RISAT-1 data having three different polarizations HH, HV and HH+HV were layer stacked to get multipolarized image. The speckle should be reduced before any further analysis of SAR images. (Lee et al. 1994) proposed several speckle reduction methods. One important aspect during the filtering process is the choice of appropriate window size. Lee et al., (1994) and Ndi Nyoungui et al., (2002) proposed some criterion to recognize the best filtering method. In this study, mean, median, mode, Lee, and Frost filters with window sizes of 3x3, 5x5, 7x7 and 9x9 were evaluated respectively. Based on relative study of filtered images by visual interpretation and time consumed for image processing, the performance of Frost and Lee methods were found similar. However, the time taken for image processing by the Frost method was found more in comparison to that of Lee

method. Therefore, the image filtered by Lee method with 5x5 window size was preferred for further analysis. The backscattering coefficient (σ°) of study area has been extracted using the Equation (2.1) (Das and Paul, 2015).

$$\sigma^{\circ}\,(\mathrm{dB}) = 20\log_{10}(\mathrm{DN_p}) - \mathrm{K_{dB}} + 10\log_{10}(\sin(\mathrm{i_p})/\sin(\mathrm{i_{center}})) \quad (2.1)$$

where σ° (dB) = SAR backscattering coefficient in dB, DN_p = digital number or the image pixel gray level count for the pixel p, K_{dB} = calibration constant in dB, i_p = incidence angle for the pixel position p, i_{center} = incidence angle at the scene center. The required values for these parameters were taken from metadata file of the image.

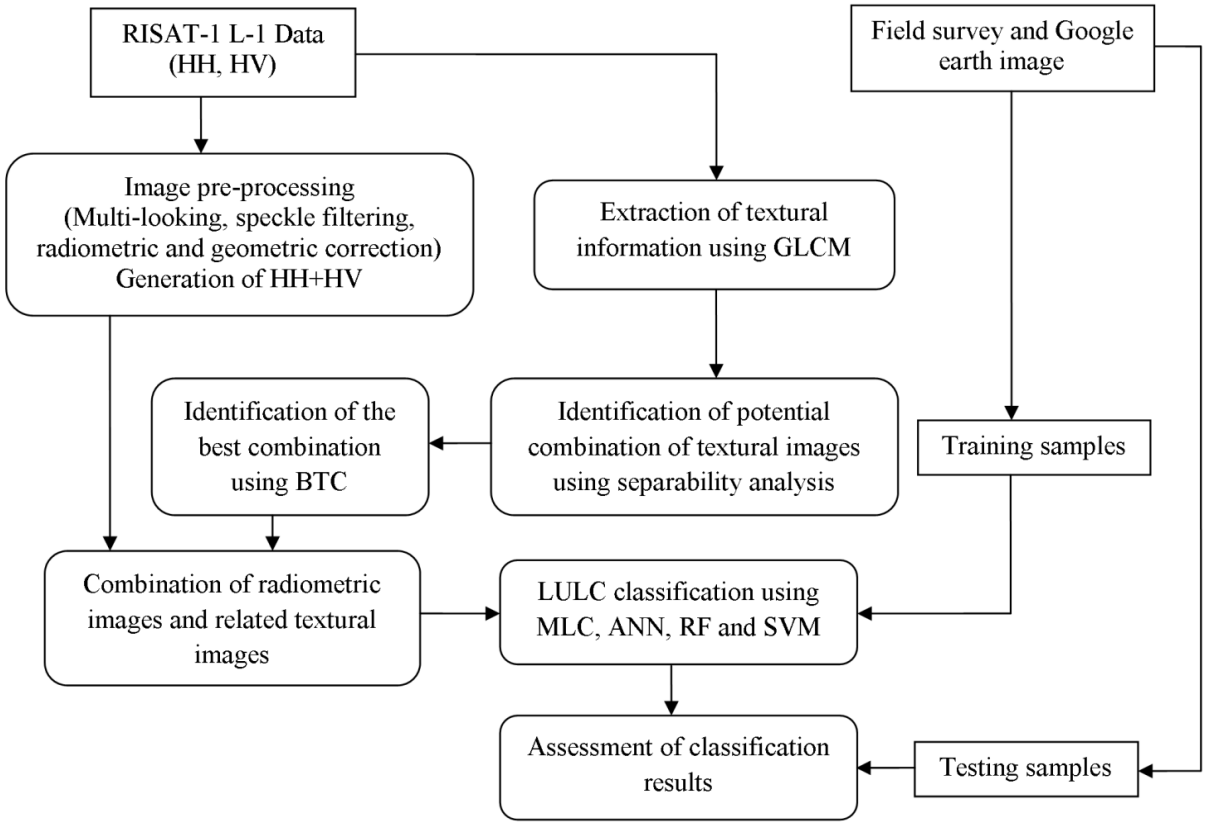

Figure 2.2 Overview of the methodology adopted for this study

The speckle filtered image was used directly for the LULC classification. In the meantime, the textural images were produced from raw SAR image by applying different

texture measures and various window sizes. The overview of methodology for this study is shown in Figure 2.2

2.3.3 Regions of interest (ROIs) and signature analyses of backscatter data of LULC classes

The samples were collected for six major LULC classes. The ROI polygons were created in the middle of respective LULC patches and well spread in the study area using ground truth information and Google earth. During field observation with hand held GPS, a total of 135 sample plots covering six LULC classes were collected. For every LULC class 20-25 sample plots were collected and each sample plot is averaged to create one signature per class for RISAT-1 image classification.

Microwave backscatter values are strongly affected by various factors such as polarization, frequency, surface roughness, and dielectric properties of the target LULC classes. To understand the backscatter behavior of various LULC classes, the scatter plot of mean backscattering coefficients (σ°) for HH and HV polarization images and number of training samples (signatures) combined per class are presented in Figures 2.3 and 2.4. It verifies that water bodies have the lowest backscatter values, while built up exhibits highest backscatter values for HH polarization image. Also, for HH polarization image sparse vegetation and fallow land are partially overlapped. Agricultural land has lower backscatter values for HH polarization than that of dense and sparse vegetation, which is primarily caused as a result of their differences in branch, stalk, and canopy cover. So, agricultural land can be separated effectively from dense and sparse vegetation by taking into account HH polarization image. Conversely, for HV polarization image, dense and sparse vegetation classes are overlapping while other classes are well separable from each other. It clearly

represents the highest and lowest backscatter values for dense vegetation and water bodies respectively. Further, to compare the differences among LULC classes, the mean and standard deviation of combined ROIs (signatures) using the HH, HV polarizations are calculated and represented in Figure 2.5.

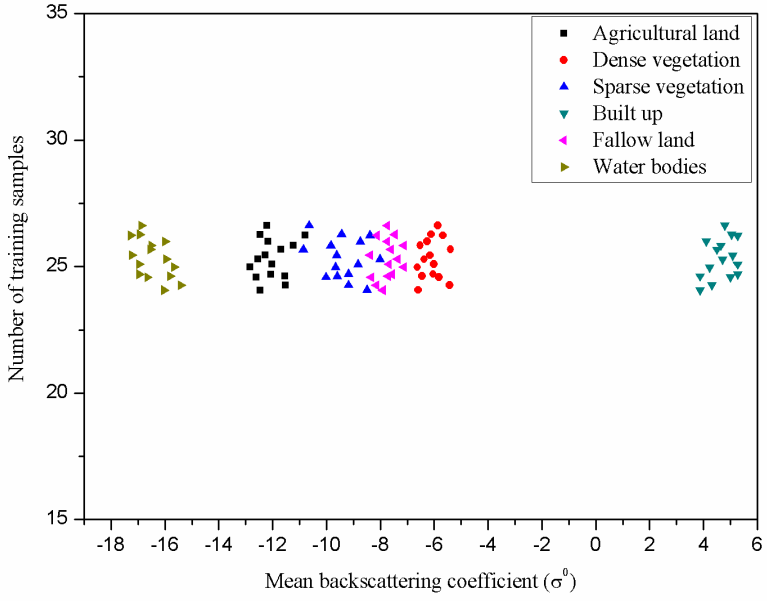

Figure 2.3 Scatter plot for HH polarization

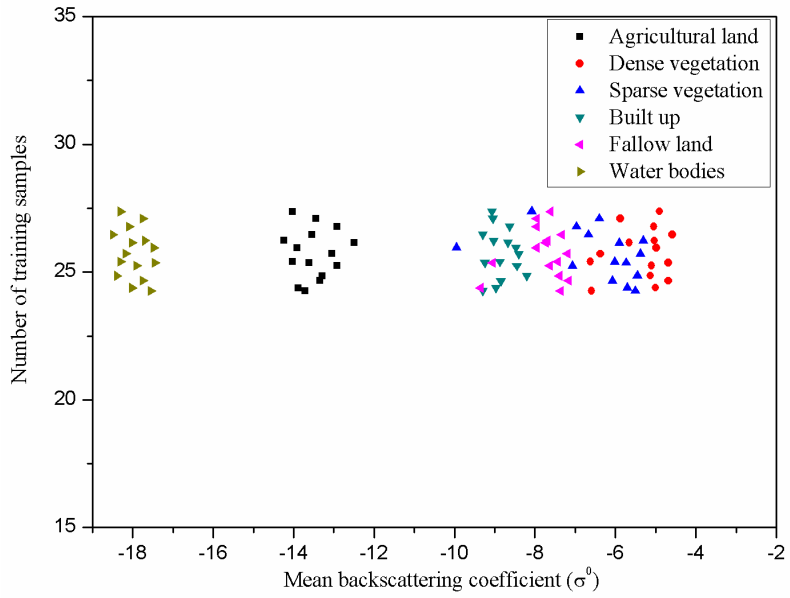

Figure 2.4 Scatter plot for HV polarization

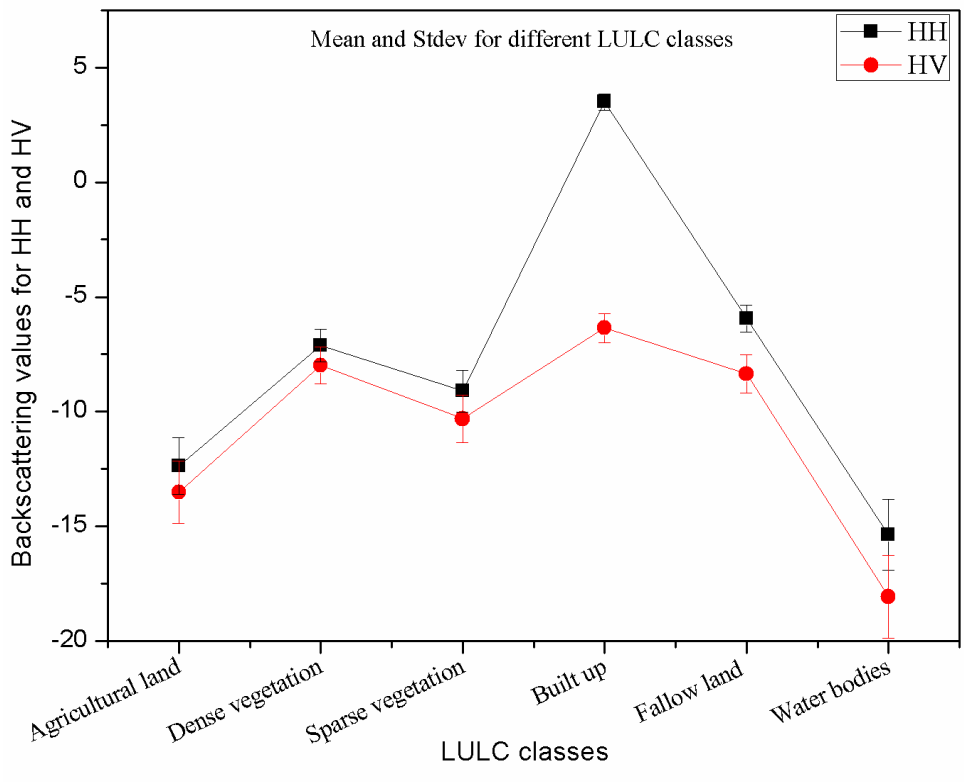

Figure 2.5 Comparison between statistical values of different LULC classes using HH and HV polarizations

2.3.4 Extraction of texture features and selection of appropriate textural images

Texture is an imperative way for the analysis of many types of images and has been broadly used to characterize diverse land features (Solberg and Jain, 1997). The most broadly used method is GLCM. Eight texture measures i.e. mean, variance, contrast, entropy, homogeneity, dissimilarity, angular second moment and correlation are frequently used in remote sensing community out of 14 originally proposed (Haralick et al., 1973). Texture analysis is found as a source to deliver important information in SAR data besides backscattering values (Luckman et al., 1997). The GLCM method is used successfully to improve LULC classification in several studies (Ndi Nyoungui et al., 2002; Herold et al., 2005). Selection of an appropriate texture feature and its most favorable window size is very

important. The extracted texture features may not characterize the common spatial pattern, if the window size is too small and it may contain other land features, if the window size is too big. Therefore, it is required to test each texture feature with a range of window sizes. Therefore, six texture features i.e. variance, contrast, entropy, homogeneity, dissimilarity, and second moment of each polarization options HH, HV and NB with seven different window sizes (3x3, 5x5, 7x7, 9x9, 11x11, 13x13 and 15x15) were extracted from GLCM for producing textural images. The texture measures and related formulae are listed in Table 1.3.

With the aim to recognize the best single and combination of textural images for LULC classification, separability analysis was carried out on the basis of different scenarios. There are a number of statistical methods available for separability analysis such as divergence, transformed divergence (TD) and Jeffreys-Matusita (JM) distance (Swain and Davis, 1978). The TD values vary from 0 to 2000 and indicate how fine the selected training samples are statistically separated. Generally, a value greater than 1900 shows a good separability, while a value less than 1700 is considered as poor separability between two LULC classes, respectively. The TD for every class pair has been calculated using the Equation (2.2) given as:

$$TD_{ij} = 2000\left(1 - \exp\left(\frac{-D_{ij}}{8}\right)\right) \quad (2.2)$$

here, D_{ij} = divergence between two signatures and can be calculated using Equation (2.3).

$$D_{ij} = \frac{1}{2}\,\mathrm{tr}\left((C_i - C_j)(C_i^{-1} - C_j^{-1})\right) + \frac{1}{2}\,\mathrm{tr}\left((C_i^{-1} - C_j^{-1})(\mu_i - \mu_j)(\mu_i - \mu_j)^T\right) \quad (2.3)$$

where i and j = the two signatures (classes) being compared, $\mathbf{C_i}$ = the covariance matrix of signature I, μ_i = The mean vector of signature I, tr = the trace function which computes the sum of the elements on the main diagonal, T = the transpose of the matrix

The class separability analysis with the help of TD method is applied to identify the potential combinations of textural images by means of the evaluation of training samples using the textural images. But for many potential combinations, the separability analysis may provide same TD values. Since all the textural images are not helpful to improve the classification accuracy. Therefore, it is necessary to develop a proper method for the selected combination of textural images to have enormous information for LULC classification. A method based on standard deviation and correlation coefficients is given as Equation (2.4) (Li et al., 2012).

$$\text{Best texture combination (BTC)} = \frac{\sum_{i=1}^{n} STD_i}{\sum_{j=1}^{n} |R_{ij}|} \quad (2.4)$$

where STD_i is the standard deviation of the textural image i, R_{ij} is the correlation coefficient between textural images i and j, n is the number of textural images.

2.3.5 LULC classification using MLC based on different scenarios

The identification of suitable polarization images and texture features for achieving the finest classification results and to investigate the performance of textural images in improving classification accuracy, different scenarios were prepared and reviewed in Table 2.1. The MLC was applied to carry out LULC classification for different scenarios. Based on the field observation and a total of 4056 pixels covering six LULC were used for image classification. The error matrix approach was utilized to appraise the classification results as discussed in section assessment of classification accuracy. Furthermore, the best identified scenario was investigated with different classifiers.

Table 2.1 Preparation of different scenarios for LULC classification using RISAT-1 data at C-band

No.	Scenarios	Examples of labels
1.	Single polarization image: HH, HV and NB (3 scenarios)	HH
2.	Combination of single-polarization images (2 scenarios)	HH&HV
3.	Textural images: selected textural images related to single polarization image (3 scenarios)	HH-text
4.	Combination of single-polarization image and appropriate textural images (3 scenarios)	HH&text
5.	Combination of textural images from different, individual polarization images (2 scenarios)	HH-&HV-text
6.	Combination of single-polarization images and their relevant textural images (2 scenarios)	HH&HV&text

Note: The sign "**-**" and "**&**" represent extracted and combination in this table. For example, HH-text means textural images extracted from HH polarization image and HH&HV means combination of HH and HV polarization images.

2.3.6 Comparison of LULC classification results using different classifiers

In the present study, four classification algorithms namely MLC, ANN, RF and SVM were employed to examine the best performed algorithm for LULC classification purpose. Same training samples were used for each classification algorithm.

2.3.6.1 MLC based classification

MLC is a most commonly used conventional supervised classification algorithm. It is based on the parametric statistical approach that entails the normal distribution of class signatures. This is a standard pixel based method based on a multivariate probability density function of classes (Lillesand et al., 2008). This method makes use of training data or class signatures captured directly from the imagery to be classified. The likelihood of a pixel

belonging to each of the classes under consideration was computed. Then the pixel is assigned a class having maximum likelihood. So, it is necessary to decide the classification plan in such a manner that each class follows a Gaussian distribution. There is limitation of MLC because of normal distribution of class signatures. Therefore, some other non parametric methods like ANN, RF and SVM have been used in this study.

2.3.6.2 ANN based classification

ANN is a mathematical technique designed to simulate functions and it is synonymic to human brain (Mas and Flores, 2008; Srivastava et al., 2012). It has capability to simulate non-linear and complex patterns with suitable topological structures (Atkinson and Tatnall, 1997). The feed forward networks which are trained by back propagation algorithm are generally used in classification of satellite images. The topological structures include three layers that is (1) a neuron in the input layer representing bands of satellite data used for classification, (2) each neuron in the output layer representing the LULC classes to be classified and (3) the hidden layer based on weighted channel connects the elements of input and output layers (Srivastava et al., 2012). For the present study, ANN have the input layer with 3 neurons indicating the bands (HH, HV and related texture feature), 1 hidden layer and 6 neurons on the output layer as six LULC classes. The rate of training was set to 0.20 and training momentum was taken as 0.90 for processing of the data by ANN. The training RMSE and training iterations were set to 0.1 and 1000 respectively. LULC classification was performed after setting all these parameters.

2.3.6.3 RF based classification

RF is an ensemble learning classification algorithm that builds many trees based on random bootstrapped samples of the training data (Breiman, 2001). Different subset from the

original training sample is applied to build each tree and the nodes are split by using the finest split variable selected out of random variables (Liaw and Wiener, 2002). Every tree adds a single vote for the assignment of the most familiar class to the input data. RF uses two parameters that is the number of trees and the number of variables used to split the nodes. The generalization error every time converges with increasing number of tress. Alternatively, a decrease in the number of predictive variables results weak individual tree. Therefore, it is recommended to choose a huge number of trees (Breiman, 2001). The samples that are not present in the bootstrap sample are known as out-of-bag (OOB) samples. The RF uses Gini index to measure the impurity of a given component with regard to the rest of the classes (Breiman et al., 1984). A higher Gini Index is more vital for discrimination. Thus, by utilizing a given combination of features, a decision tree is made to develop to its utmost depth with no pruning.

2.3.6.4 SVM based classification

SVM is a non-parametric machine learning technique, primarily constructs an optimal separating hyperplane between the linearly separable classes within a multidimensional feature space. It is designed to maximize the margin between optimal separating hyperplane and closest training samples called "support vectors" (Vapnik, 1998). In general, larger the margin, lower the generalization error of the classifier. The optimization algorithms are used by SVM to locate the optimal decision boundaries between the classes. SVM uses linear decision boundaries for linearly distinguishable classes. If there are non-linearly separable classes, the idea of kernel is to develop to handle the classification problems (Cortes and Vapnik, 1995).

The radial basis function (RBF) kernel was found most appropriate choice for the present study. Because, it needs less computational work and can handle the non linear relationship between the training samples and the entire data set.

The function $K(x_{i,}x_j) = \phi(x_i)^T \phi(x_j)$ is named as the kernel function and C > 0 is the penalty parameter. Here the training vectors x_i are mapped into a space with higher dimension by the function ϕ. The RBF kernel is given by Equation (2.5).

$$\text{Radial basis function} : K(X_i, X_j) = \exp\left(-\gamma \left\| (X_i, X_j) \right\|^2\right), \gamma > 0 \quad (2.5)$$

For RBF kernel, two parameters namely penalty parameter (C) and gamma parameter (γ) were set to as default values. The value of pyramid parameter was set to be zero to process the image at full resolution.

2.3.7 Assessment of classification accuracy

The assessment of classification accuracy is based on the parameters UA, PA, OA, and Kc and related formulae was given by equations (1.1) to (1.4). For more comprehensive assessment of classification results, F-measure (Puissant et al., 2014) was calculated for individual class using equation (1.5). In the present study, a total of 1352 pixels were collected during the field observations which were applied for accuracy assessment for each LULC class.

The Z-test was also carried out to assess significant differences between the classification results obtained by different classifiers (Foody, 2009). It is a statistical test of the difference in accuracy measures by comparing kappa coefficients. The value of Z-test is obtained by using the Equation (2.6)

$$Z = \frac{\widehat{K}_1 - \widehat{K}_2}{\sqrt{\widehat{\sigma}^2{}_{K_1} + \widehat{\sigma}^2{}_{K_2}}} \quad (2.6)$$

where $\widehat{K}_1$and $\widehat{K}_2$ are the calculated kappa coefficients for the classification outputs obtained from two different classification methods, and $\widehat{\sigma}^2{}_{K_1}$ and $\widehat{\sigma}^2{}_{K_1}$ show the corresponding variances (Foody, 2009). Therefore, $|Z| >$ 1.96 will show that the two compared classification measures (error matrices) are significantly different at the 5% significance level. The number of training and testing pixels used for the classification purpose are presented in Table 2.2.

Table 2.2 Number of pixels in each class type used for training and testing of MLC, ANN, RF, and SVM algorithms

	Agricultural land	Dense vegetation	Sparse vegetation	Built up	Water bodies	Fallow land	Total
Number of training pixels	765	705	720	690	696	480	4056
Number of testing pixels	255	235	240	230	232	160	1352

2.4 RESULTS AND DISCUSSION

2.4.1 Identification of suitable polarization and textural images

The separability analysis performed by using training samples indicates that a single polarization image such as HH, HV or NB cannot classify the diverse LULC classes effectively. As the average TD values for all LULC class pairs based on training sample plots of different classes for HH and HV images were only 1765 and 1720. The separability was improved for a combination of HH and HV images and average TD value became greater than 1900. This study reveals the fact that the radiometric data is not adequate to separate different LULC classes effectively. So, it is required to produce new images to improve classification accuracy. Such new images can be produced with the help of texture measures

by using the spatial information contained in the image. Table 2.3 represents the textural images having average TD values greater than 1900.

There are 42 textural images based on six texture measures and seven different window sizes for each polarization images such as HH, HV and NB. The separability analysis performed with the help of TD method shows that the ability of most of the single textural images is poor to separate different LULC classes. The textural images having average TD values over 1900 are listed in Table 2.3. For both HH and HV images, the window size of 7x7 was found best for texture analysis. However, the window size of 9x9 was found best for the NB image. Depending on different polarization images, the best texture measure was found varying. The TD analysis demonstrates that the single textural images are not able to separate diverse LULC classes effectively. There are numerous possible combinations of two textural images on a single polarization image. The TD analysis based on two textural images exhibits that the combination of two textural images may improve the LULC class separation. The potential textural images with higher TD values over 1900 obtained with the help of training samples are summarized in Table 2.3. For HH image, textural image based on dissimilarity with 7x7 window size and homogeneity with 3x3 window size gave the best result. For HV image, textural image based on contrast with 3x3 window size and homogeneity with 3x3 window size gave the best result. The combination of second moment with 3x3 window size and entropy with 9x9 window size provided the best results for the NB image. The potential combination of textural images for each polarization images are presented in Table 2.3.

Table 2.3 Identification of textural images used for LULC classification

RISAT-1 C-band	Single textures	Combinations	Best texture combination
HH	DIS9, HOM3,DIS5	DIS5-CON3, DIS7-HOM3, DIS7-CON3, CON5-DIS9	DIS7-HOM3
HV	CON3, DIS9, CON5, HOM3	HOM5-DIS9, CON3-HOM3, CON5-HOM3	CON3-HOM3
NB	SM3, ENT13	ENT9-ENT13, SM3-ENT9	SM3-ENT9

Note: Variance (VAR), Homogeneity (HOM), Contrast (CON), Dissimilarity (DIS), Entropy (ENT), Second moment (SM) is the texture features listed in Table 1.1. The number with each texture feature indicates the window size.

2.4.2 Comparison of LULC classification results among scenarios

The relative appraisal of the accuracy of classification results using MLC among single polarization images, textural images corresponding to the polarization images and combinations of single polarization images and associated textural images are represented in Tables 2.4, 2.5 and 2.6 respectively. It clearly shows that HH and NB images performed better than HV image for LULC classification. The textural images derived from NB image are superior to those of HH and HV images. The combination of single polarization images and related textural images provided improved classification accuracy by 6.06-10.94% in comparison to single polarization images. It also revealed that NB image did not give improved classification accuracy than HH image, but the textures derived from NB image improved the classification accuracy than textures derived from HH and HV images.

The LULC classification results on the basis of combination of different polarization images, textural images and their combinations are presented in Table 2.7. The combination of HH and HV polarization images, the combination of their corresponding textural images,

or the combination of both polarization images and textural images improved accuracy significantly for LULC classification in contrast to individual polarization images or associated textural images. The combination of HH and HV polarization images or combination of HH, HV and NB reduced the classification accuracy because of the poor performance of individual polarization images in LULC classification. However, the incorporation of NB derived textural images is very useful for improving classification accuracy. The combination of HH, HV, NB and their corresponding textural images gave the best classification result with kappa coefficient 0.755 which is slightly better than the combination of HH, HV and their corresponding textural images with kappa coefficient 0.737. The combination of HH, HV and their corresponding textural images or the combination of HH, HV, NB and their corresponding textural images provided the best classification results with OA of 78.18% and 79.65% respectively as shown in Table 2.7. For the combination of HH, HV and their corresponding textural images, the UA ranged from 67.86 to 82.72 % while the PA ranged from 59.38 to 86.64%. While for the combination of HH, HV, NB and their corresponding textural images, the UA ranged from 73.94 to 83.05% and the PA ranged from 65.63 to 85.78% for all LULC classes. The UA and PA values for all other combinations of HH and HV, or HH, HV, and NB and their corresponding textural images are represented in Table 2.7.

Table 2.4 MLC based comparison of LULC classification results among the individual band, textural images, and the combination of individual band and related textural images for HH polarization image

LULC Class	HH		HH-text		HH&text	
	PA (%)	UA (%)	PA (%)	UA (%)	PA (%)	UA (%)
Agricultural land	50.98	53.50	58.43	60.32	61.57	62.55
Dense vegetation	57.45	51.33	61.28	55.38	64.26	60.16
Sparse vegetation	57.92	50.55	62.08	58.66	64.58	61.26
Built up	52.61	59.02	58.70	61.09	62.61	65.75
Water bodies	66.81	59.85	60.34	62.78	64.22	65.64
Fallow land	53.13	58.21	55.00	59.86	56.88	60.26
OA (%)	56.58		59.54		62.64	
Kc	0.494		0.512		0.550	

Table 2.5 MLC based comparison of LULC classification results among the individual band, textural images, and the combination of individual band and related textural images for HV polarization image

LULC Class	HV		HV-text		HV&text	
	PA (%)	UA (%)	PA (%)	UA (%)	PA (%)	UA (%)
Agricultural land	45.10	50.44	49.80	52.70	52.94	56.96
Dense vegetation	53.19	49.21	57.02	53.17	60.85	58.37
Sparse vegetation	54.58	49.06	56.25	54.88	59.17	57.03
Built up	51.30	57.56	56.09	58.11	60.87	63.35
Water bodies	64.22	56.87	62.50	61.18	64.22	62.87
Fallow land	49.38	52.31	53.75	55.84	56.88	55.83
OA (%)	53.03		55.91		59.17	
Kc	0.432		0.469		0.508	

Table 2.6 MLC based comparison of LULC classification results among the individual band, textural images, and the combination of individual band and related textural images for NB polarization image

LULC Class	NB		NB-text		NB&text	
	PA (%)	UA (%)	PA (%)	UA (%)	PA (%)	UA (%)
Agricultural land	47.84	51.91	60.78	65.13	64.71	66.27
Dense vegetation	54.04	49.61	65.11	59.07	65.96	62.75
Sparse vegetation	56.25	49.09	65.42	63.31	67.08	67.93
Built up	52.61	59.02	64.78	64.78	65.65	68.33
Water bodies	65.09	57.41	62.50	65.32	68.10	68.10
Fallow land	50.63	58.21	57.50	59.35	59.38	57.23
OA (%)	54.51		62.94		65.45	
Kc	0.449		0.553		0.584	

Table 2.7 MLC based comparison of LULC classification results based on different combinations of HH and HV, or HH, HV, and NB and their combinations with corresponding textural images

LULC class	HH&HV		HH-&HV-text		HH&HV&text		HH&HV&NB		HH-&HV-&NB-text		HH&HV&NB&text	
	PA (%)	UA (%)	PA (%)	UA (%)	PA (%)	UA (%)	PA (%)	UA (%)	PA (%)	UA (%)	PA (%)	UA (%)
Agricultural land	61.96	67.52	63.53	69.23	72.55	77.08	63.14	70.00	65.10	71.55	74.51	81.20
Dense vegetation	70.64	65.10	72.77	66.54	80.43	79.08	74.47	72.31	76.60	71.71	82.98	81.25
Sparse vegetation	67.50	61.83	70.42	67.60	80.00	78.37	70.42	71.31	72.92	73.84	81.67	83.05
Built up	66.06	74.15	68.70	71.82	84.78	79.59	78.70	72.69	80.43	78.06	83.48	76.80
Water bodies	68.53	65.16	72.41	72.10	86.64	82.72	81.03	77.05	81.90	80.17	85.78	79.60
Fallow land	60.63	58.21	63.13	63.92	59.38	67.86	55.63	59.33	63.13	63.92	65.63	73.94
OA (%)	66.12		68.71		78.18		71.22		73.74		79.65	
Kc	0.592		0.623		0.737		0.653		0.684		0.755	

2.4.3 Comparison of LULC classification results using different algorithms

The classified products achieved by using different algorithms are shown in Figure 2.6 (a-d). ANN, RF and SVM were found to improve the OA of LULC classification with respect to MLC. For accuracy assessment, the error matrices are produced for the classified results using MLC, ANN, RF and SVM algorithms. The highest OA 88.97% was achieved by SVM in comparison to those of RF, ANN and MLC algorithms with 88.45%, 83.65% and 78.18% respectively. The Kc values 0.867, 0.860, 0.803 and 0.737 were also achieved for four different algorithms namely SVM, RF, ANN and MLC respectively. The UA, PA, OA, Kc and F-measure statistics achieved using four different classification algorithms are presented in Table 2.8. The UA ranged from 67.86 to 82.72%, 71.71 to 88.98%, 77.56 to 92.83% and 79.11 to 92.98%, while PA ranged from 59.38 to 86.64%, 68.13 to 90.52%, 76.10 to 97.00% and 78.13 to 96.98% for MLC, ANN, RF and SVM algorithms respectively. Evaluation of classification accuracy regarding to F-measure is higher for SVM in comparison to RF, ANN and MLC. It ranged from 63.33 to 84.63%, 69.87 to 89.74%, 76.83 to 94.76% and 78.62 to 94.94% for MLC, ANN, RF and SVM respectively.

The Z-test was utilized by comparing confusion matrices to test whether the two classification results were significantly different or not. The classification results indicate that the combinations SVM vs. MLC and SVM vs. ANN have given Z values more than 1.96, while SVM vs. RF provides Z value less than 1.96. It means that SVM vs. MLC and SVM vs. ANN were found to be significantly different, but SVM vs. RF was observed to be insignificantly different. It was found that SVM vs. RF, SVM vs. ANN and SVM vs. MLC combinations given Z values 1.46, 7.27 and 13.82 respectively. Critically, SVM resulted in 0.52% increase in OA than the RF which was statistically insignificant or statistically no difference was found between

classification accuracies. The classified maps indicate that there is mixing between the built up and dense vegetation. The dense vegetation is overestimated in MLC then ANN, RF and SVM. Some part of agricultural land is misclassified as dense and sparse vegetation by MLC algorithm. The SVM, RF and ANN provided the OA more than 80% however; the lower OA (78.18%) achieved by the MLC algorithm shows fair agreement between the classified image and ground truth data.

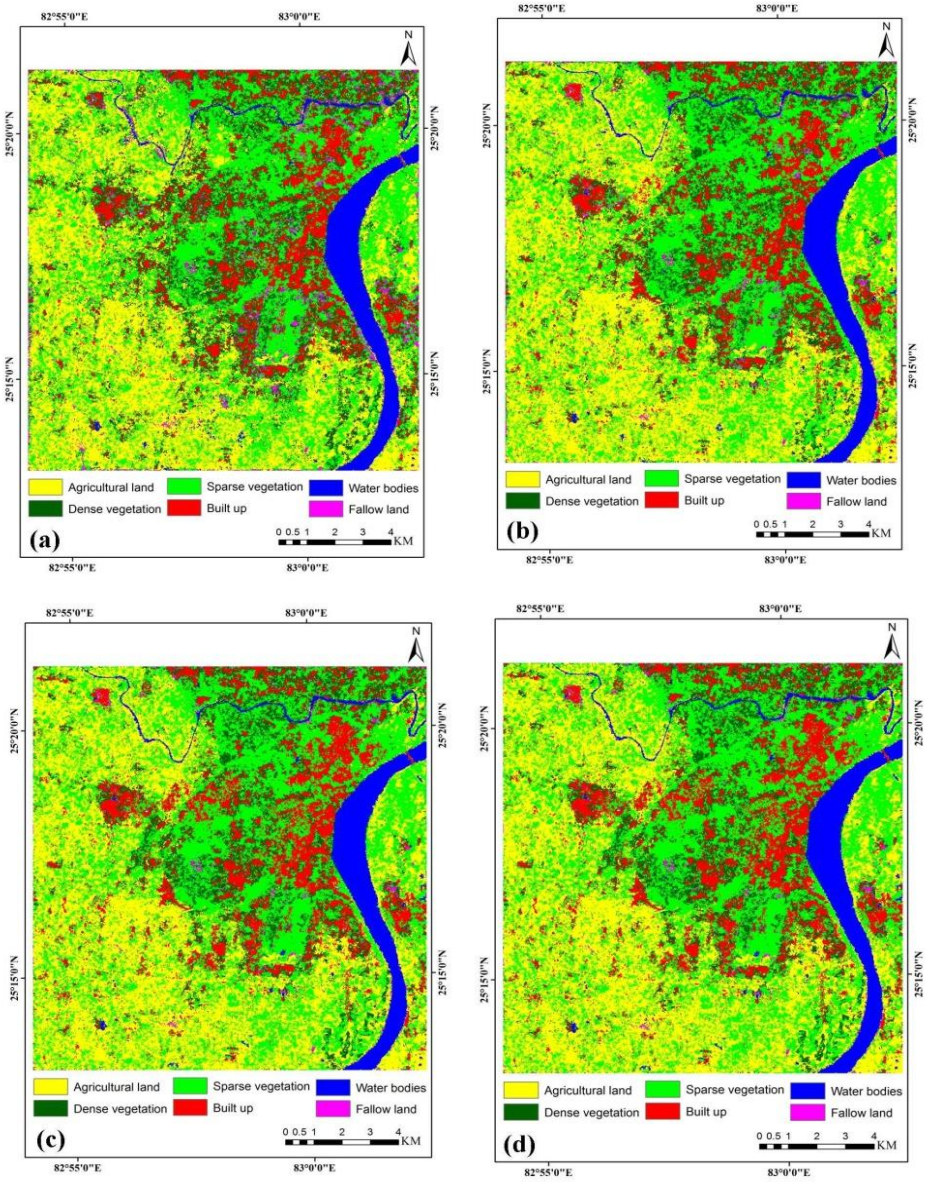

Figure 2.6 Classified LULC maps based on (a) MLC, (b) ANN, (c) RF, and (d) SVM algorithms

Table 2.8 Comparison of LULC classification results obtained from different classification algorithms based on the combinations of HH, HV, and corresponding textural images

LULC class	MLC			ANN			RF			SVM		
	PA (%)	UA (%)	F-measure (%)	PA (%)	UA (%)	F-measure (%)	PA (%)	UA (%)	F-measure (%)	PA (%)	UA (%)	F-measure (%)
Agricultural land	72.55	77.08	74.75	77.65	84.26	80.82	83.53	88.75	86.06	84.31	89.58	86.87
Dense vegetation	80.43	79.08	79.75	86.38	87.12	86.75	87.98	87.98	87.98	88.09	88.46	88.27
Sparse vegetation	80.00	78.37	79.18	85.00	83.95	84.47	87.87	87.14	87.50	87.92	87.55	87.73
Built up	84.78	79.59	82.11	90.00	81.82	85.71	94.83	92.83	93.82	95.65	92.83	94.22
Water bodies	86.64	82.72	84.63	90.52	88.98	89.74	97.00	92.62	94.76	96.98	92.98	94.94
Fallow land	59.38	67.86	63.33	68.13	71.71	69.87	76.10	77.56	76.83	78.13	79.11	78.62
OA (%)	78.18			83.65			88.45			88.97		
Kc	0.737			0.803			0.860			0.867		

2.5 CONCLUSION

The present study explored LULC classification of SAR data and usefulness of the integration of radiometric and textural information in improving classification accuracy. The dual polarimetric C-band RISAT-1 data was utilized for LULC classification using texture features extracted using GLCM method. MLC algorithm provided convincingly good classification accuracies for six major LULC classes with OA of 78.18% and Kc 0.737. In comparison to MLC, the classifiers ANN, RF and SVM performed better in improving OA by 5.74%, 10.27% and 10.79% respectively. It is concluded as well that the texture features varies with the different polarization images. However, the best window sizes were found to be 7x7 and 3x3 for HH and HV images respectively, whereas it was 9x9 for NB image. In the case of a single polarization image, the HH image performed better than HV and NB images. The textural images derived from HH, HV and NB images performed better in comparison to their related radiometric images. Also, the textural images derived from NB image and the combination of NB image and their corresponding textural images performed still better than that of HH and HV images.

The combinations of different polarizations and their resultant textural images done by adding NB image into HH and HV improved the classification accuracy in contrast to the combination of HH and HV images. The combination of HH, HV, NB and their corresponding textural images performed slightly better than that of HH, HV and related textural images. On the basis of above discussions, it is concluded that the LULC classification of SAR data is a difficult task. However, this study may be very useful when there is unavailability of optical data due to clouds. Furthermore, the investigation of SAR

data or integration of SAR and optical data can also be performed for improving accuracy in LULC classification.